

Polymer shape anisotropy and the depletion interaction

Mario Triantafillou and Randall D. Kamien

Department of Physics and Astronomy, University of Pennsylvania, Philadelphia, Pennsylvania 19104

(Received 7 December 1998)

We calculate the second and third virial coefficients of the effective sphere-sphere interaction due to polymer-induced depletion forces. By utilizing the anisotropy of a typical polymer conformation, we can consider polymers that are roughly the same size as the spheres. We argue that recent experiments are laboratory evidence for polymer shape anisotropy. [S1063-651X(99)01705-5]

PACS number(s): 61.25.Hq, 36.20.Ey, 82.70.Dd

Over 60 years ago, Kuhn studied the conformations of polymer chains [1] and recognized that typical conformations of ideal chains are *not* spherically symmetric. The intuitive idea of a symmetric shape is a result of the isotropic end-to-end vector distribution of a random walk [2]: spherical symmetry results from implicit rotational averaging of the polymer. In fact, a typical polymer conformation is anisotropic, with an aspect ratio of roughly 3.4:1 [3].

Nonetheless, there is little laboratory evidence for this asphericity. In solution, polymers rotate randomly and there are no significant polymer-polymer correlations. Thus small angle light-scattering measurements of polymer solutions can only determine the average principal axis of the polymer shape. If there were a way to induce strong orientational correlations, light-scattering measurements could discern an asymmetry. We will show that the induced attraction between regions of depleted polymer concentration (inclusions) is a probe of this shape anisotropy.

The shape tensor characterizes the spatial distribution of monomers:

$$M_{\alpha\beta} = \int_0^N dn [R_\alpha(n) - \bar{R}_\alpha][R_\beta(n) - \bar{R}_\beta], \quad (1)$$

where $R_\alpha(n)$ is the position of monomer n , α and β label the Cartesian coordinates, and $\bar{R}_\alpha \equiv (1/N) \int_0^N dn R_\alpha(n)$ is the polymer center of mass. The polymer radius of gyration is simply $R_G^2 = \text{Tr}(M)$. Moreover, the eigenvalues of $M_{\alpha\beta}$, $\lambda_1^2 \leq \lambda_2^2 \leq \lambda_3^2$, are the average squared radii of gyration along the principal axes of inertia. Simulations [3,4] have determined that the most likely shape has

$$\lambda_3^2 : \lambda_2^2 : \lambda_1^2 \approx 11.8 : 2.7 : 1.0. \quad (2)$$

Indeed, the shape asymmetry exists and is rather large [5]. Exploiting this shape anisotropy as a calculational tool is the main theoretical component of this paper.

Though hard spheres only interact by direct contact, entropic effects of other particles present can induce long-range interactions. These sorts of forces are responsible for liquid-crystalline order in lyotropic systems [6] and surface crystallization in hard-sphere fluids [7]. It is instructive to consider the virial expansion for a gas of identical balls. Around each sphere of radius r there is a sphere of radius $2r$ from which the centers of the other spheres are excluded. When two spheres are close, their excluded regions overlap leaving

more free volume for the remaining spheres and hence a larger entropy. Thus the propensity for “close” configurations can be interpreted as an entropic “depletion” force.

Recently [9], monodisperse polymers (specifically λ -phage DNA) have been used to induce depletion forces between polystyrene spheres. To model this system at low concentrations, one might replace the polymers with spheres of radius R_G , the polymer radius of gyration. Asakura and Oosawa derived a simple formula for the potential between two large spheres of diameter σ in a gas of smaller spheres of diameter D . The Asakura-Oosawa (AO) potential is [8]

$$\frac{U(R)}{k_B T} = \frac{\Pi v \lambda^3}{(\lambda - 1)^3} \left[1 - \frac{3}{2} \left(\frac{R}{\sigma \lambda} \right) + \frac{1}{2} \left(\frac{R}{\sigma \lambda} \right)^3 \right], \quad (3)$$

where R is the distance between the centers of the large spheres, v is the volume of a small sphere, Π is the osmotic pressure of the small-sphere gas, and $\lambda \equiv 1 + D/\sigma$. The above approximation simply sets $D = 2R_G$. This is obviously a crude approximation to the true system. A complete analysis at length scales longer than the polymer persistence length (50 nm) would count the number of self-avoiding random walks which avoid the two polystyrene spheres.

In general, the effective potential is of the form $U_{\text{eff}} = \Pi V(R)$ where Π is the osmotic pressure and V is an R -dependent recovered volume. At low concentrations the osmotic pressure is not adjustable: $\Pi = k_B T c$. The physics all lies in $V(R)$. The AO model gives a one-parameter family of functions, depending on the effective hard-sphere diameter D . In principle one could derive a virial expansion for this potential with each term involving the evaluation of a set of cluster integrals, each of which involves integrations over polymer degrees of freedom. We will derive a different one-parameter family based on the known shape distribution of polymers and argue that the data in [9] are the first laboratory evidence of the conformational anisotropy.

We start by calculating the classical configurational integral $Q_N(R)$, the sum of Boltzmann weights over all conformations of N polymers with two spherical inclusions separated by R . The sphere-sphere effective potential $U_{\text{eff}}(R)$ is

$$P(R) = \frac{Q_N(R)}{\int d\mathbf{R} Q_N(R)} \equiv \frac{\exp\{-\beta U_{\text{eff}}(R)\}}{\int d\mathbf{R} \exp\{-\beta U_{\text{eff}}(R)\}}. \quad (4)$$

Although $Q_N(R)$ has terms which are independent of R , the resulting effective potential $U_{\text{eff}}(R)$ does not: they cancel between numerator and denominator in Eq. (4).

To calculate $Q_N(R)$, we sum over all the conformations and placements of N polymers with the excluded-volume Boltzmann weights: 1 if the polymers and the spheres do not overlap and 0 otherwise. We split the integration over each polymer into three parts. The first is an integration over the center of mass, the second an integration over all rigid rotations of the conformation, while the third is the remaining integration over ‘‘internal’’ degrees of freedom. This final integral is over each unique conformation — two conformations are equivalent if one is merely a rigid rotation or translation of the other. We will only integrate over one representative from each equivalency class. Denoting the space of all such ‘‘internal’’ polymer conformations by Y , we have

$$Q_N = \frac{1}{N!} \prod_{i=1}^N \int_Y dr_{i,\text{int}} \int d\mathbf{r}_i d\Omega_i e^{-\beta U}, \quad (5)$$

where $dr_{i,\text{int}}$ is the measure on the space of conformations for polymer i , \mathbf{r}_i is its center of mass, and Ω_i is its rigid rotation. We further divide the integration over Y by characterizing each polymer conformation by its principal axes. Defining $g(\lambda_1, \lambda_2, \lambda_3)$ as the number of conformations with axes λ_i , we have

$$Q_N = \frac{1}{N!} \prod_{i=1}^N \int d\lambda_{i1} d\lambda_{i2} d\lambda_{i3} g(\lambda_{i1}, \lambda_{i2}, \lambda_{i3}) \times \int d\mathbf{r}_i d\Omega_i e^{-\beta U}. \quad (6)$$

To pass from Eq. (5) to Eq. (6) we assumed that the internal degrees of freedom did not affect the interaction potential U . This is, of course, not precisely correct. Our approximation replaces each polymer by a solid ellipsoid, and then considers the potential due only to this shape. While this certainly removes many degrees of freedom, it includes more degrees of freedom than replacing the polymers by spheres. We will see that this approximation is valid by comparison with data [9]. Thus our approximation replaces the monomer-sphere and monomer-monomer potential with a sum of pairwise, ellipsoid-ellipsoid, or sphere-ellipsoid terms. Each term is infinite for any overlap and zero otherwise.

We now reduce the complexity of the integration in Eq. (6) by using the shape distribution of polymers. Since the distribution of polymer shapes is peaked around the prolate spheroid, we *only* consider those polymer shapes. This approximation does not account for the entire space of principal axes, though we believe that it does characterize the polymer conformations better than a sphere. More importantly, our approximation allows us to consider polymers which are roughly the same size as the included spheres. This has a great advantage when comparing to the experiments of Verma *et al.* [9]. By comparison, most work in this field has treated the inclusions approximately while correctly modeling the medium as a gas of random walkers. In [10] field theoretic methods were used to obtain the depletion potential. There, in order to calculate reliably, the authors

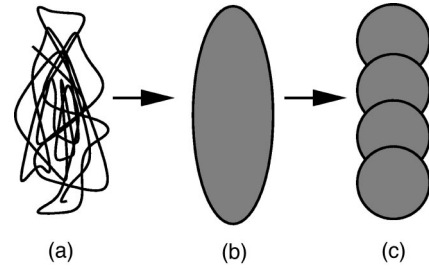


FIG. 1. Sequence of approximations. The actual polymer performs a self-avoiding random walk (a) which has a typical prolate spheroidal shape (b). For computational simplicity, we neglect the anisotropy between the two shorter principal axes and build up the resulting ellipsoid out of overlapping spheres (c).

considered the interaction between inclusions much smaller than the polymers, i.e., $\sigma \ll R_G$. In the opposite extreme, one might consider polymers which are much smaller than the spheres. In this case, it is appropriate to study the induced Casimir force between two walls and to then approximate the interaction between spheres via the Derjaguin approximation [11]. By approximating the polymers as prolate spheroids, we can treat the inclusions exactly — a great advantage when the two extreme limits are not applicable.

We have thus reduced the configurational integral Q_N over all polymer modes to an integral over the allowed locations and orientations of a prolate spheroid. In order to reduce the phase space somewhat and reduce our computation time, we will assume that $\lambda_1 = \lambda_2$. In the case of interest, we consider a prolate spheroid with aspect ratio $\sqrt{11.8}:1 \approx 3.4:1.0$, so that

$$g(\lambda_1, \lambda_2, \lambda_3) \propto \delta(\lambda_1 - \lambda_2) \delta[\lambda_3 - (3.4)\lambda_1] \times \delta(R_G^2 - [2\lambda_1^2 + \lambda_3^2]), \quad (7)$$

where R_G is the radius of gyration of the polymer. To facilitate the numerical evaluation of integrals, we construct the ellipsoid out of overlapping spheres. Figure 1 depicts our sequence of approximations. We note that choosing $\lambda_3 \gg \lambda_2 = \lambda_1$ would reduce our analysis to that in [12] which considered the depletion force between two spheres induced by thin rods.

Writing $f_{ij} = e^{-\beta u_{ij}} - 1$, where u_{ij} is the excluded-volume potential between particles i and j , and labeling the spheres A and B , $Q_N(R)$ can be rewritten as

$$Q_N = \frac{1}{N!} e^{-\beta u_{AB}} \int_V d\mathbf{r}_1 d\Omega_1 d\mathbf{r}_2 d\Omega_2 \cdots d\mathbf{r}_N d\Omega_N \times (1 + f_{A1})(1 + f_{B1})(1 + f_{A2})(1 + f_{B2})(1 + f_{12}) \cdots \quad (8)$$

The product in Eq. (8) is a sum of terms which can be grouped by the number of polymer positions and rotations that are freely integrated over. The first term is proportional to $(4\pi V)^N$, the configurational integral for free ellipsoids, where V is the volume of space minus the volume of the two included spheres. Subsequent terms have fewer powers of V . Since the polymers are identical, these corrections include

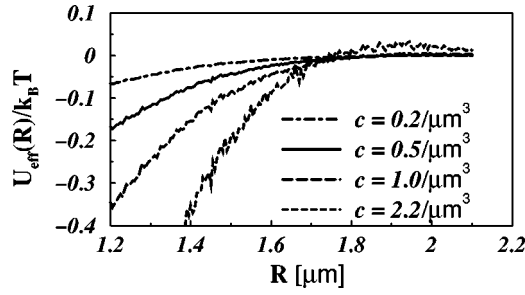


FIG. 2. Numerical result for the effective potential U_{eff} for differing concentrations and $R_G = 0.5 \mu\text{m}$. We have kept terms up to second order in the polymer concentration. Note that at the highest concentration there is a small repulsive bump at $R \approx 2 \mu\text{m}$. However, for $c \leq c^* \approx 2/\mu\text{m}^3$, the third virial coefficient is a small contribution to U_{eff} .

combinatoric factors involving N . We take the limit $N \rightarrow \infty$ and $V \rightarrow \infty$ keeping $c \equiv N/V$ constant to find the virial expansion in c .

It is both convenient and instructive to graphically represent these ‘‘cluster’’ integrals [13] in terms of Mayer cluster graphs. The first two terms in $U_{\text{eff}}(R)$ are

$$\beta U_{\text{eff}}(R) = \frac{c}{4\pi} \int d\mathbf{r}_1 d\Omega_1 \mathcal{L} + \frac{1}{2} \left(\frac{c}{4\pi} \right)^2 \times \int d\mathbf{r}_1 d\mathbf{r}_2 d\Omega_1 d\Omega_2 \left[2\mathcal{T} + 2\mathcal{K} + 2\mathcal{N} + 2\mathcal{R} + \mathcal{X} \right] \quad (9)$$

where the open dots represent the spherical inclusions and the closed dots represent the ellipsoids. The integrals in Eq. (9) are difficult to compute analytically and thus were evaluated numerically via a Monte Carlo algorithm: 10^3 different angles and 10^4 different points were chosen in a volume which included both spheres and which did not exclude any possible orientation or location of the ellipsoids. We calculated these integrals by this random sampling weighted by the appropriate phase-space volume factor.

To compare with experiment [9], we took the sphere diameter to be $D = 1.2 \mu\text{m}$ and $R_G = 0.5 \mu\text{m}$. Knowing R_G enables us to find the length of the ellipsoid, $L = 3.4 \times 2R_G / \sqrt{13.8} \approx 0.92 \mu\text{m}$. We have chosen the hard-ellipsoid radii to be the mean square radii of gyration, which is possibly naive: the hard-ellipsoid size should only be proportional to R_G . Since in a random walk the density decays as $1/r$, there is no natural length scale which cuts off the excluded-volume interaction. Indeed, light-scattering experiments [14] have found that the effective hard-sphere radius is roughly half the radius of gyration. The relation between R_G and the hard-ellipsoid size must be determined through the depletion-force experiments we are modeling.

In Fig. 2 we plot our results as a function of concentration. Until one considers concentrations near the polymer overlap concentration $c^* = 1/(4\pi R_G^3/3) \approx 2/\mu\text{m}^3$, the third virial coefficient, responsible for a repulsive ‘‘anti-correlation hole,’’ is a small perturbation to the leading term in Eq. (9). Thus if we restrict our study to the dilute polymer regime, the leading term in the virial expansion is sufficient.

We compare our model with the data [9] and the AO model at $c = 0.5/\mu\text{m}^3$ for two reasons. This concentration is

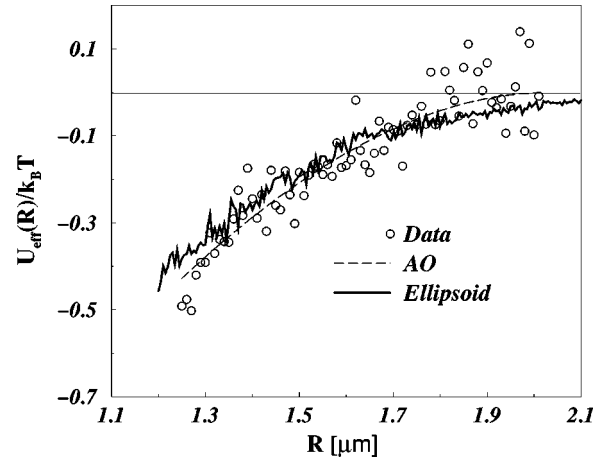


FIG. 3. Our model and the AO model are fit to the experimental data for $c = 0.5/\mu\text{m}^3$. We varied only the effective R_G as a parameter. The fit gives $R_G = 0.42$ and 0.8 for the AO model, and our model, respectively.

below the overlap concentration c^* and at the same time is large enough that the well depth is on the order of $k_B T$ so that data can be reliably obtained. We can adjust the effective radius R_G for both the AO model and our ellipsoid-based model. We find that a good fit results for the AO model with $R_G = 0.42 \mu\text{m}$ and for our model with $R_G = 0.8 \mu\text{m}$, in comparison with the light-scattering-obtained value $R_G = 0.5 \mu\text{m}$. In Fig. 3 we show the data along with these two one-parameter fits. We have checked other concentrations and have found that at $c = 1.0/\mu\text{m}^3$ the theory and experiment also compare favorably with the same effective radii. What should one conclude from this agreement? It is possible to interpret the data as arising from either shape simply by adjusting the size of the shape. However, one should start from a microscopic picture based on the polymer physics of the allowed chain conformations. Only from this perspective can one properly interpret the data.

Since the radius of gyration of the λ -DNA can be calculated from its molecular weight and persistence length to be $R_G = 0.5 \mu\text{m}$, we can consider two different zero parameter fits: our model and the AO model. The result is shown in Fig. 4. Note that the data lie between our calculation and the

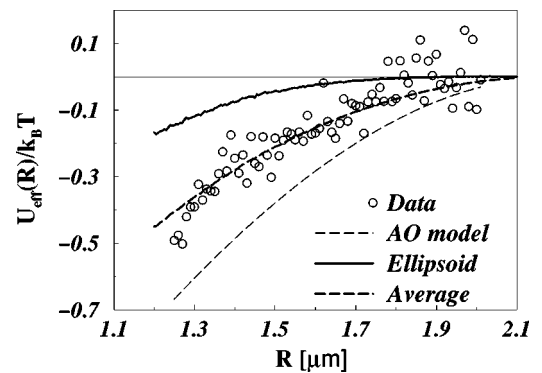


FIG. 4. Comparison of the AO model, the model presented here, and the data at $c = 0.5/\mu\text{m}^3$. For both our model and the AO model we have taken the theoretical value of $R_G \approx 0.5 \mu\text{m}$. There are no free parameters in the models. We also plot the average of the AO model and the ellipsoid calculation.

AO model, suggesting that one could smoothly deform the AO sphere into an ellipsoid and find a best-fit aspect ratio to fit the data, giving a one-parameter fit. Indeed, we have made a number of limited runs on the fully anisotropic shape satisfying Eq. (2). This results in a curve which is roughly 30% deeper than that in Fig. 4, which is better than the simple spherocylinder result. Finally, we have made similar comparisons between theory and experiment at $c=0.1/\mu\text{m}^3$, $c=0.2/\mu\text{m}^3$, and $c=1.0/\mu\text{m}^3$. We find that at $c=1.0/\mu\text{m}^3$ the comparison is similar to that shown in Fig. 4. At the two lower concentrations, where the data are difficult to collect, neither our model nor the AO model make very good predictions.

Returning to the original question, are polymer shapes anisotropic? Though the full distribution $g(\lambda_1, \lambda_2, \lambda_3)$ is peaked, it has a finite width. We can incorporate this width by choosing an appropriately weighted admixture of shapes. Note that we could easily get a very good fit just by mixing spheres and ellipsoids — the mixed second virial coefficient is just a linear combination of the two “pure” coefficients. It is easy to see from Fig. 4 that a 50-50 admixture of spheres

and ellipsoids would give a remarkably good fit to the data, without any adjustable parameters. While we have no basis for this weighting of shapes, we nonetheless take this as direct evidence for the anisotropy of polymer conformations.

In closing, we note that while counting polymer conformations by treating them as rigid ellipsoids is appropriate for static properties, it is not clear at all that the dynamics reflects this. In particular one might ask whether a polymer ellipsoid rotates to a new orientation slower or faster than it deforms into that orientation. Finally, our analysis could also be used to study the depletion interaction by actual ellipsoidal objects, such as bacteria [15].

It is a pleasure to acknowledge conversations with J. Crocker, D. Discher, A. Levine, T. Lubensky, D. Pine, R. Verma, and A. Yodh. We additionally thank the authors of [9] for providing us with their data. This research was supported in part by the Research Corporation, the Donors of The Petroleum Research Fund, administered by the American Chemical Society, and the NSF-MRSEC Program through Grant No. DMR96-32598.

-
- [1] W. Kuhn, *Kolloid-Z.* **68**, 2 (1934).
 [2] M. Doi and S.F. Edwards, *The Theory of Polymer Dynamics* (Oxford University Press, Oxford, 1986), p. 29.
 [3] K. Šolc, *J. Chem. Phys.* **55**, 335 (1971).
 [4] D.E. Kranbuehl and P.H. Verdier, *J. Chem. Phys.* **67**, 361 (1977).
 [5] We note that although polymer self-avoidance leads to a swelling of the polymer chain, it does not significantly alter the shape anisotropy. See J.A. Aronovitz and D.R. Nelson, *J. Phys. (Paris)* **47**, 1445 (1986).
 [6] M. Adams, Z. Dogic, S.L. Keller, and S. Fraden, *Nature (London)* **393**, 349 (1998).
 [7] A.D. Dinsmore, A.G. Yodh, and D.J. Pine, *Nature (London)* **383**, 239 (1996).
 [8] S. Asakura and F. Oosawa, *J. Chem. Phys.* **22**, 1255 (1954).
 [9] R. Verma, J. Crocker, T.C. Lubensky, and A.G. Yodh, *Phys. Rev. Lett.* **81**, 4004 (1998).
 [10] A. Hanke, E. Eisenriegler, and S. Dietrich, e-print cond-mat/9808225.
 [11] J.F. Joanny, L. Leibler, and P.-G. de Gennes, *J. Polym. Sci., Polym. Phys. Ed.* **17**, 1073 (1979); see also Y. Mao, M.E. Cates, and H.N.W. Lekkerkerker, *J. Chem. Phys.* **106**, 3721 (1997).
 [12] K. Yaman, C. Jeppesen, and C.M. Marques, *Europhys. Lett.* **42**, 221 (1998).
 [13] See, for instance, R.K. Pathria, *Statistical Mechanics* (Butterworth-Heinemann, New York, 1996).
 [14] X. Ye, T. Narayanan, P. Tong, and J.S. Huang, *Phys. Rev. Lett.* **76**, 4640 (1996).
 [15] We thank D. Discher for discussions on this point.